Osthole attenuates angiogenesis in an orthotopic mouse model of hepatocellular carcinoma via the downregulation of nuclear factor-κB and vascular endothelial growth factor

FEI YAO[1], LURONG ZHANG[1,2], GUORONG JIANG[1,2], MIN LIU[1], GUOQIANG LIANG[1] and QIN YUAN[1]

[1]Laboratory of Clinical Pharmacy of Chinese Herb, Suzhou Hospital of Traditional Chinese Medicine, Suzhou, Jiangsu 215000; [2]Laboratory of Clinical Pharmacy of Chinese Herb, Suzhou Academy of Wumen Chinese Medicine, Suzhou, Jiangsu 215003, P.R. China

Received December 1, 2017; Accepted June 27, 2018

DOI: 10.3892/ol.2018.9213

Abstract. Osthole has been demonstrated to have antitumor activity. Previous studies by our group indicated that osthole effectively inhibited tumor growth in hepatocellular carcinoma (HCC) through the induction of apoptosis and enhancement of antitumor immune responses in mice. The importance of angiogenesis in the proliferation, invasion and metastasis of tumor cells in HCC is well established. The present study aimed to investigate the effects of osthole on angiogenesis in an orthotopic mouse model of HCC. Orthotopic HCC in mice was established, and osthole at 61, 122 and 244 mg/kg was administered intraperitoneally once daily to the tumor-bearing mice for 14 consecutive days. Immunohistochemistry was performed to analyze the microvessel density (MVD) of tissues, and the level of vascular endothelial growth factor (VEGF) was measured by ELISA. The protein levels of nuclear factor-κB (NF-κB) p65 and IκB-α were also detected by western blotting. MVD was positively correlated with tumor weight in the orthotopic mouse model of HCC. Osthole administration significantly decreased MVD in tumor and adjacent tissues, and inhibited tumor growth. Furthermore, osthole downregulated the expression of VEGF and NF-κB p65, and upregulated IκB-α expression in tumor and adjacent tissues. To the best of our knowledge, the results of the present study demonstrated for the first time that osthole inhibits angiogenesis in an orthotopic mouse model of HCC, which may be one of the mechanisms underlying the anti-HCC activity of osthole, which in turn may be mediated by the NF-κB/VEGF signaling pathway. Therefore, osthole, a potential angiogenesis inhibitor and immune system enhancer, may be a promising lead compound for the treatment of HCC.

Correspondence to: Dr Lurong Zhang or Dr Guorong Jiang, Laboratory of Clinical Pharmacy of Chinese Herb, Suzhou Hospital of Traditional Chinese Medicine, 18 Yangsu Road, Suzhou, Jiangsu 215000, P.R. China
E-mail: suzhouzlr2013@163.com
E-mail: szguorongjiang@163.com

Key words: osthole, hepatocellular carcinoma, angiogenesis, microvessel density, nuclear factor-κB, vascular endothelial growth factor

Introduction

Angiogenesis is a key event in the promotion of cancer, being a process required for tumor cell proliferation, invasion and metastasis (1-3). Hepatocellular carcinoma (HCC) has been recognized to be a hypervascular tumor, and its prognosis is associated with angiogenesis (4). A number of anti-angiogenesis drugs have been approved by the US Food and Drug Administration and are being used in cancer therapy (5). In the treatment of HCC, anti-angiogenic therapy is considered among the most promising strategies. However, in clinical practice, anti-angiogenic therapy alone appears to be insufficient for improving patient survival, for overcoming the occurrence of resistance and for producing enduring clinical responses (6,7). Furthermore, immunosuppression occurs as a result of the establishment of hypoxia during anti-angiogenic therapy, and thus anti-angiogenic drugs are typically used in combination with chemotherapeutic and immune-enhancing agents (7-10). Therefore, the identification of an anti-angiogenic lead compound with the properties of minimal toxicity and immunoprotection that may serve as a natural chemopreventative agent is becoming increasingly important (11).

Osthole, 7-methoxy-8-(3-methyl-2-butenyl) coumarin, is a bioactive coumarin derivative that may be extracted from a number of medicinal plants, including *Cnidium monnieri* (L.) Cusson. It has a history of use in traditional Chinese medicine for the treatment of eczema, cutaneous pruritus, trichomonas vaginalis infection and sexual dysfunction. More recent studies have revealed that osthole possesses antitumor effects by inhibiting tumor cell growth and inducing apoptosis (12-15). Previous studies by our group have demonstrated that osthole may effectively inhibit tumor growth in various HCC cell lines and models with no or minimal toxicity via the induction of apoptosis, and in tumor-bearing mice with HCC, via the enhancement of antitumor immune responses mediated by T cells (16,17). However, it is currently unknown whether osthole has anti-angiogenic activity in HCC.

Anti-angiogenic drugs aimed at blocking vessel growth in cancer are based on the targeting of vascular endothelial growth factor (VEGF)-VEGF receptor (VEGFR) signaling (5,18). A high level of VEGF expression has been identified in HCC (19). Nuclear factor-κB (NF-κB) has been reported to be a critical regulator of the VEGF pathway (20). When cells are stimulated by external factors, they trigger a series of enzyme-linked reactions. The activation of NF-κB promotes tumor necrosis factor (TNF)-α to produce VEGF and positively regulate the expression of mRNA and proteins in the VEGF pathway (21). A previous study by our group also identified that osthole significantly suppressed NF-κB activity in a time- and dose-dependent manner in hepatoma cells (16).

In the present study, an orthotopic mouse model of HCC was established, and the effects of osthole on microvessel density (MVD) in tumor and adjacent tissues, and on tumor growth were examined to investigate its potential anti-HCC role as an inhibitor of angiogenesis; furthermore, the effects of osthole on the expression of NF-κB and VEGF in the tumor and adjacent tissues was determined to examine the potential mechanism underlying its anti-angiogenic effect.

Materials and methods

Chemicals and reagents. Osthole ($C_{15}H_{16}O_3$;molecular weight, 244.29; purity, ≥99%) was purchased from National Institutes for Food and Drug Control, Beijing, China and dissolved in corn oil prior to use. All other chemicals and reagents were purchased from Sigma-Aldrich; Merck KGaA (Darmstadt, Germany).

Cell culture. The murine HCC Hepa1-6 cell line was a gift from Dr Limin Zheng (School of Life Sciences, Sun Yat-Sen University, Guangzhou, China). Cells were maintained in high glucose Dulbecco's modified Eagle's medium (DMEM; Gibco; Thermo Fisher Scientific, Inc., Waltham, MA, USA), supplemented with 10% heat-inactivated fetal bovine serum (Gibco; Thermo Fisher Scientific, Inc.) at 37˚C in a humidified atmosphere containing 5% CO_2.

Animal model and treatment. The male C57/BL6 mice [n, 88; age, 6-8 weeks; weight, 20-22 g; provided by the animal experiment center of Matt Albert Technology Co., Ltd., Suzhou, China; animal certificate no. SCXK (JING) 2014-0004] were used for the establishment of an orthotopic mouse model of HCC following adaptive feeding for 3 days. An orthotopic transplanted model of murine HCC was established as described by previous studies (22,23). The model was induced by intrahepatic implantation of $2x10^6$ Hepa1-6 cells into the left liver lobes of mice, and the animals were maintained in laminar flow cabinets under pathogen-free conditions, and Small Animal Diagnostic Ultrasound (IVIS Lumina; Cold Spring Harbor Laboratory, Cold Spring Harbor, NY, USA) was performed at early and late time points to confirm the presence of a tumor and for assessment of tumor burden (24). When the tumor weight reached >10% of the body weight of the experimental mice, the mice were sacrificed by cervical dislocation. All experimental protocols and procedures were performed in accordance with the EU Directive 2010/63/EU for animal experiments. The present study was approved by the Local Ethics Committee of Suzhou Hospital of Traditional Chinese Medicine (Suzhou, China). The mice were administrated with osthole according to programme A and B.

Programme A was as follows: The mice bearing tumors at 8 days that were in the initial tumor stages were randomly distributed into five groups and each group consisted of 8 mice. They were treated with 61 mg/kg (0.25 mmol/kg), 122 mg/kg (0.5 mmol/kg) and 244 mg/kg (1.00 mmol/kg) osthole intraperitoneally (i.p.) in 0.2-ml corn oil, with corn oil alone as the model control group and cisplatin (5 mg/kg; Qilu Pharmaceutical Co., Ltd., Jinan, China) as the chemotherapy control once every other day for 2 weeks. Programme B was as follows: The mice bearing tumors at 13 days that were at the rapid growth stage of the tumor were randomly distributed into five groups and each group consisted of 8 mice. The mode of administration was the same as that of Programme A. Additionally, 8 C57BL/6 mice without tumor cell inoculation were treated with corn oil alone as the normal control group.

Assessment of tumor weight. A total of 24 h after the last treatment administration at day 14, mice were sacrificed. The tumor tissues and adjacent tissues were weighed and collected. Tumor inhibition rate (%)=(mean tumor weight of model control group-mean tumor weight of experiment group)/mean tumor weight of model control group x100.

Immunohistochemistry (IHC) assay and analysis. Tumor and adjacent tissue specimens from the harvested livers were fixed for 24 h at 25˚C in 4% formalin followed by embedding in paraffin. Tissue sections (4-μm thick) were subjected to IHC. For deparaffinization, sections were washed in xylene for 5 min each a total of three times, then in two washes of 100% ethanol for 10 min each, in two washes of 95% ethanol for 10 min each and washed sections twice in dH_2O for 5 min each. For antigen retrieval, slides were brought to a boil in 10 mM sodium citrate buffer, (pH 6.0) and maintained at a sub-boiling temperature for 10 min and cooled for 30 min. In order to block endogenous peroxidase blocking, sections were incubated in 3% hydrogen peroxide for 10 min and were washed in dH_2O twice for 5 min each, and blocked each section with 100-150 μl blocking solution (1% w/v BSA, TBS) for 2 h at 25˚C. The sections were subjected to staining procedures with purified monoclonal anti-rabbit CD34 primary antibody (dilution, 1:250; cat. no. ab81289; Abcam, Cambridge, UK) at 4˚C overnight. Subsequently, biotinylated goat anti-rabbit immunoglobulin secondary antibodies (dilution, 1:2,000; cat. no. ab205718; Abcam, Cambridge, UK) was incubated for 1 h at 25˚C. Rabbit specific HRP conjugate (cat. no. D110117; Sangon Biotech Co., Ltd., Shanghai, China) was incubated for 15 min at 25˚C. The visualization signals were developed using 3,3'-diaminobenzidine chromogen substrate (Boster Biological Technology, Pleasanton, CA, USA) and the slides were counterstained with Meyer's hematoxylin for 1~2 min at 25˚C and dehydrated through ethanol and xylene series (25). The sections were observed with a light microscope (Nikon Corporation, Tokyo, Japan) at x200 magnification.

ImageJ software (version 1.8.0; National Institutes of Health, Bethesda, MD, USA) was used to quantify MVD based on CD34 staining. The percentage of positively stained

area was calculated using a color deconvolution for separating the staining components in ≥5 fields per section (26). The results are presented as the percentage of the treated group compared with the model or normal group. All sections were analyzed and evaluated independently by two double blinded pathologists (ZL and YQ), and the results were reconfirmed when inconsistent.

ELISA assays of VEGF expression in tumor and adjacent non-tumor tissues. Tumor and adjacent non-tumor liver tissue specimens of HCC-bearing mice treated with corn oil or osthole were homogenized on ice with PBS (50 mg tissue and 500 μl PBS). Homogenates were centrifuged at 3,000 x g for 10 min at 4˚C and the supernatants (100 ml) were used for analysis. The concentrations of VEGF in the tissue homogenate were quantitatively measured using commercially available ELISA kits (cat. no. 110518007; eBioscience; Thermo Fisher Scientific, Inc.) according to manufacturer's protocols.

Western blot analysis. Liver tumor and adjacent tissues were lysed on ice using nuclear protein and cytosolic protein extraction kits (Beyotime Institute of Biotechnology) for 30 min. The lysates were centrifuged at 14,000 x g for 10 min at 4˚C and supernatants were collected. The nuclear proteins were quantified using a bicinchoninic acid protein assay kit (Beyotime Institute of Biotechnology). Equal amount of protein (100 μg) were loaded onto 10% SDS-PAGE and transferred onto polyvinylidene difluoride membranes. The membranes were blocked with 5% skimmed dried milk buffered for 2 h at 25˚C and incubated with primary antibodies against NF-κB p65 rabbit mAb (dilution, 1:1,000; cat. no. 0009; Cell Signaling Technology, Inc., Danvers, MA, USA) and IκB-α antibody (dilution, 1:1,000; cat. no. 0010; Cell Signaling Technology, Inc.) overnight at 4˚C. Next, the membranes were washed and incubated with horseradish peroxidase-conjugated Goat Anti-Rabbit IgG [H+L] secondary antibody (dilution, 1:2,000; cat. no. 0822WB; Cell Signaling Technology, Inc.) for 2 h at 25˚C. Blots were washed four times with tris-buffered saline with Tween-20 and detected by a fluorescence visible imaging system (ProteinSimple, San Jose, CA, USA), according to the manufacturer's protocol. The quantification was normalized to the corresponding value of GAPDH (dilution, 1:1,000; cat. no. 0006; Cell Signaling Technology, Inc.) expression used ImageJ software (version 1.8.0; National Institutes of Health, Bethesda, MD, USA).

Statistical analysis. All data represent ≥3 independent experiments and the results of the experimental studies are expressed as the mean ± standard error of the mean. Statistical significance of differences was analyzed using the Student's t-test or one-way analysis of variance, followed by the Bonferroni's or Dunnett's post hoc tests, and correlation analysis was assessed using Pearson's correlation coefficient. Statistical analyses were performed using GraphPad Prism 5.0 Software (GraphPad Software, Inc., La Jolla, CA, USA). $P<0.05$ was considered to indicate a statistically significant difference.

Results

Osthole suppresses tumor growth in orthotopic HCC-bearing mice. To establish an orthotopic mouse model of HCC, HCC Hepa1-6 cells were injected into the left liver lobes of mice. As demonstrated in Fig. 1A, the mice developed internal liver tumors. Subsequently, the antitumor effects of osthole on an orthotopic mouse model of HCC were studied throughout different stages of tumor growth. On days 8 and 13 after the establishment of tumor xenografts (via programmes A and B, respectively), the mice were treated intraperitoneally with osthole at 61, 122 and 244 mg/kg for 2 weeks, with corn oil treatment as the model control and cisplatin treatment (5 mg/kg) as the positive control. The mean tumor weight of programme A mice in the model control group was 220.60±19.05 mg, and of programme B mice was 2,390.80±232.57 mg. Compared with the model control group, the osthole treatment groups (61, 122 and 244 mg/kg) exhibited significantly suppressed tumor growth ($P<0.01$); the tumor inhibition rates of osthole at 61, 122 and 244 mg/kg were 27.02, 45.24 and 68.09%, respectively, in the programme A mice, and 21.58, 50.31 and 59.21%, respectively, in the programme B mice (Fig. 1A). These results demonstrated that osthole inhibited tumor growth in orthotopic HCC-bearing mice.

Additionally, in the present study, cisplatin treatment decreased body, thymus and spleen weight in orthotopic HCC-bearing mice ($P<0.01$), whereas treatment with osthole had no effect on body, thymus and spleen weight in the mice (Fig. 1B-D). This indicated that osthole exerted no apparent toxicity in the orthotopic HCC-bearing mice, which was similar to the model treatment.

Osthole suppresses angiogenesis in the tumor tissues of orthotopic HCC-bearing mice. Based on the antitumor effect of osthole, the effect of osthole on angiogenesis in tumor tissue was subsequently determined. Programmes A and B were used to investigate the effects of osthole on the different stages of blood vessel development in the process of tumor growth. IHC for CD34 expression was performed on tumor tissue specimens. Compared with the model control group, MVD in the HCC tissues of the osthole treatment groups was significantly decreased ($P<0.05$ and $P<0.01$; Fig. 2A and B). Furthermore, MVD in HCC tissues was increased during the progression of tumor growth, and MVD was correlated with tumor weight ($r=0.6314$, $P<0.01$; Fig. 2C). These data suggested that osthole suppressed angiogenesis in the tumor tissues of orthotopic HCC-bearing mice.

Effects of osthole on VEGF and NF-κB signaling in the tumor tissues of orthotopic HCC-bearing mice. The NF-κB-mediated VEGF signaling pathway (NF-κB/VEGF) has been reported to be one of the mechanisms regulating tumor angiogenesis (4,27). Therefore, the present study determined the expression levels of VEGF and NF-κB in HCC tumor tissues. The effects of osthole on the expression of VEGF in the tumor tissues were analyzed by ELISA. The concentration of VEGF in tumor tissue homogenate was 13.17±3.51 ng/ml in the programme A tumor-bearing mice and 16.01±9.63 ng/ml in the programme B tumor-bearing mice (Fig. 3A). Compared with the model control treatment, osthole decreased the expression of VEGF in tumor tissues ($P<0.05$; Fig. 3A). To further elucidate the molecular basis of the anti-angiogenic effect of osthole, the effect of osthole on NF-κB activity was investigated. The protein expression of IκB-α and NF-κB p65 was detected by

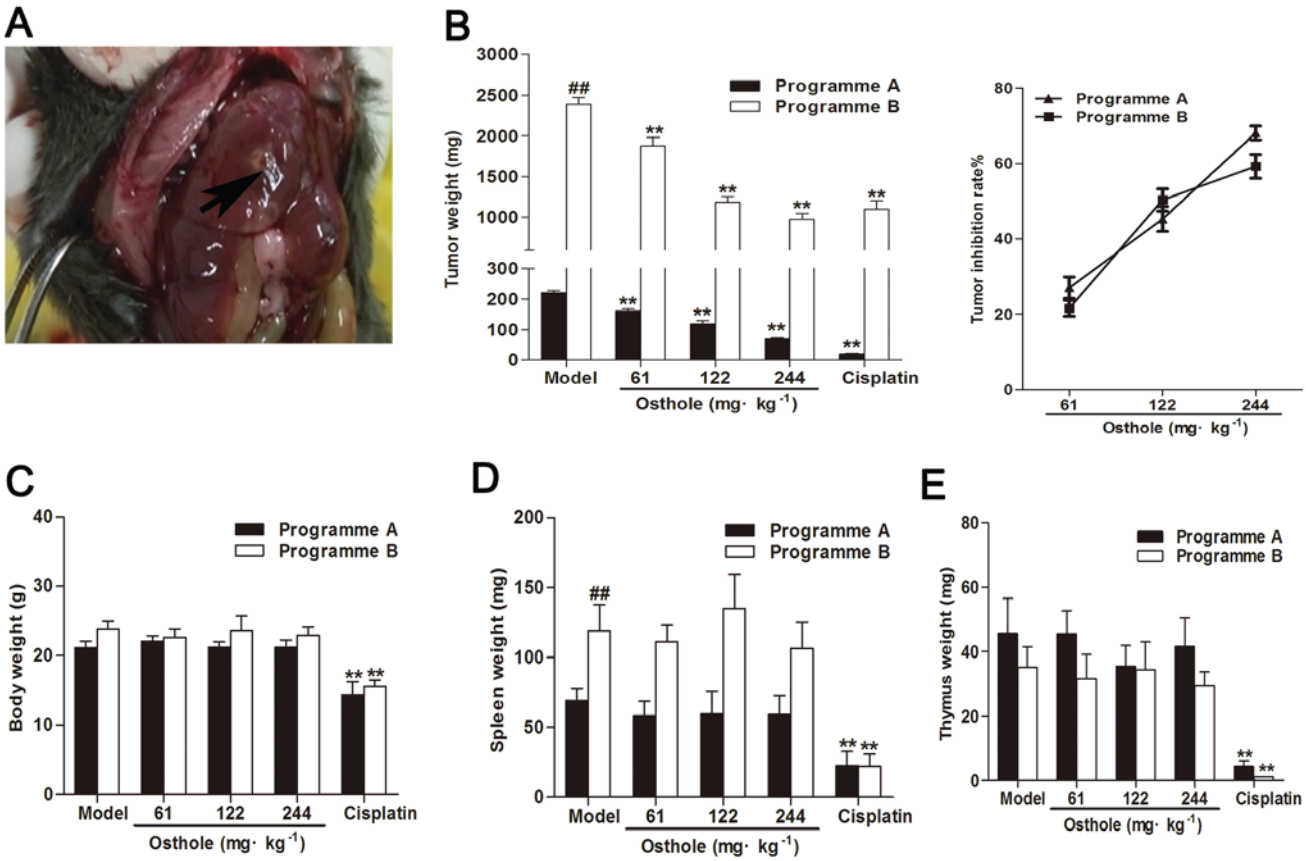

Figure 1. Osthole suppresses tumor growth in orthotopic HCC-bearing mice. (A) A total of $2x10^6$ Hepa1-6 cells were injected into the left liver lobes of C57/BL6 mice (arrow). (B) Tumor weights of the C57/BL6 mice inoculated with Hepa1-6 cells and treated with osthole 14 days. The tumor inhibition rate of osthole was calculated. The (C) body weights, (D) spleen weights and (E) thymus weights of the C57/BL6 mice inoculated with Hepa1-6 cells were weighed on day 14. Each data point represents the mean ± standard error of the mean of 8 mice. **P<0.01, compared with the model control group; $^{\#\#}$P<0.01, compared with programme B model control group.

western blot analysis. Compared with the model control treatment, the expression of IκB-α was increased, while that of NF-κB p65 was decreased, in tumor tissues following osthole treatment (P<0.01; Fig. 3B). Taken together, these results demonstrated that the downregulation of NF-κB and VEGF was involved in the anti-angiogenesis effect of osthole in the tumor tissues of orthotopic HCC-bearing mice.

Effects of osthole on MVD, and VEGF and NF-κB signaling in the adjacent tissues of orthotopic HCC-bearing mice. Within the tumor microenvironment, the interaction of malignant tumor cells and non-malignant cells makes the microenvironment supportive for the growth of the tumor (28). It has been identified that the components of the tumor microenvironment serve an important role in the development of tumor angiogenesis and may modulate tumor angiogenesis in various ways (29). In the present study, IHC results showed that there was no expression of CD34-positive microvessels in normal liver tissue (Fig. 4A). Adjacent tissue was a distance of 0.5 cm from the tumor tissue. Compared with the normal control group, MVD in the adjacent tissues of the model control group was significantly increased (P<0.01; Fig. 4B), the expression of VEGF was marginally increased (normal, 20.67±2.13 ng/ml; model, 23.43±1.37 ng/ml; Fig. 4C) and the levels of IκB-α were decreased while those of NF-κB p65 were increased (P<0.05; Fig. 4D). The upregulation of NF-κB and VEGF expression in adjacent tissues was consistent with the development of HCC.

Compared with the model control group, MVD in the adjacent tissues of the osthole-treated groups exhibited a decreasing trend (Fig. 4B) and the expression of VEGF was also decreased (P<0.01; Fig. 4C). Additionally, western blot analysis revealed that the expression levels of IκB-α were increased while those of NF-κB p65 were decreased in the adjacent tissues with osthole treatment (P<0.05; Fig. 4D). These data were consistent with the effects of osthole on the tumor tissues.

Discussion

The aim of the present study was to investigate the effect of osthole on the inhibition of angiogenesis in an orthotopic mouse model of HCC. A novel finding of the present study was that osthole inhibited angiogenesis in the orthotopic mouse model of HCC in a dose-dependent manner. Furthermore, in tumor and adjacent tissues, it was noted that osthole not only downregulated the expression of VEGF, but also reduced NF-κB activity, which supported the anti-angiogenesis effect of osthole. Additionally, it was also demonstrated that osthole inhibited tumor growth in the orthotopic mouse model of HCC in a dose-dependent manner. The results of the present study suggested that the anti-angiogenesis effect of osthole participates in its suppression of tumor growth.

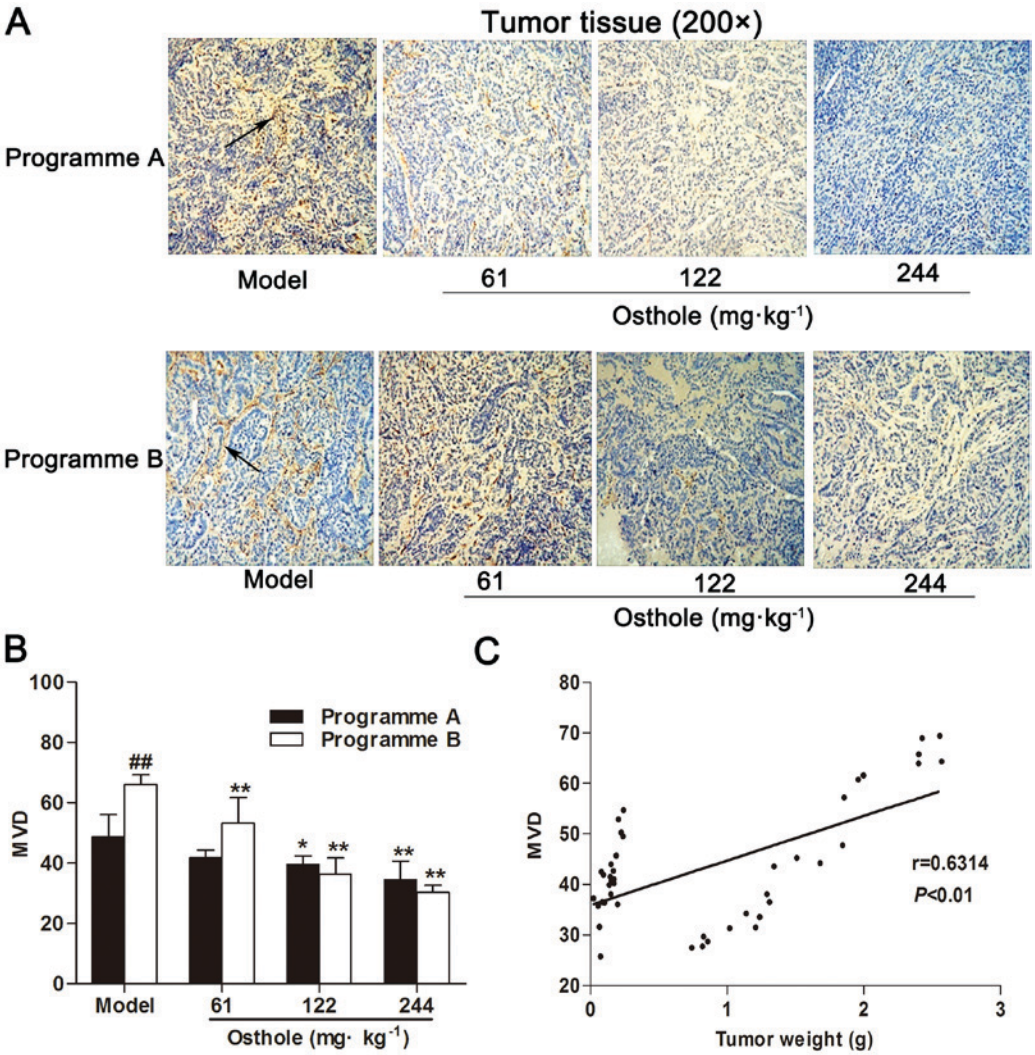

Figure 2. Osthole suppresses angiogenesis in tumor tissues of orthotopic hepatocellular carcinoma-bearing mice. (A) Immunohistochemical staining for blood vessels with CD34 (arrow) was performed on tumor tissues from osthole-treated (61, 122 and 244 mg/kg) mice. (B) Compared with the model control group, the staining indicates that MVD was significantly decreased in the osthole-treated mice. (C) Tumor weight was correlated with MVD (P<0.01; r=0.6314). Data are presented as the mean ± standard error of the mean. *P<0.05, **P<0.01, compared with the model control group. $^{\#\#}$P<0.01, compared with the programme A model control group. MVD, microvessel density.

HCC mouse models are currently established by chemical induction, transgenesis and transplantation, with orthotopic transplantation mouse models considered optimal for imitating the growth of tumors and observing tumor morphology and microenvironment (30,31). The orthotopic mouse model of HCC can be established by the injection of HCC cells or the tumor tissues into the mouse liver, and the growth of tumors can be monitored using imaging techniques (24,32,33). The present study directly injected the HCC Hepa1-6 cell line into the left liver lobes of mice to generate internal liver tumors, and Small Animal Diagnostic Ultrasound was performed at early (7 or 8 days) and late (20-27 days) time points to confirm the presence of a tumor and for the assessment of tumor burden, respectively. In the present study, it was observed that the maximum ratio of tumor weight (2.571 g) to body weight (26.1 g) was 9.85%, indicating that the orthotopic mouse model of HCC was appropriate. The present study established the orthotopic mouse model of HCC to investigate neovascularization in tumor and adjacent tissues, as well as its association with tumor growth. At the initial stage of tumor growth (7 or 8 days after injection of hepatoma cells), intratumoral neovascularization was mostly absent, while at the rapid growth stage of HCC (12 or 13 days after injection of hepatoma cells), intratumoral neovascularization was abundant. A relatively high dose of osthole was used based on our previous study that aimed to achieve therapeutic effects, in which osthole-treated mice exhibited no apparent signs of toxicity. The current orthotopic mouse model exhibited similar reactions to the xenograft HCC model in our previous study (16). In the present study, similarities and differences in the effects of osthole on the growth and angiogenesis of tumor tissues at the initial and rapid growth stages of tumor development were observed. MVD may be involved in the ability of tumor tissue to induce angiogenesis (34). CD34 is considered to be a sensitive and specific marker of microvessels in HCC (35). The present study examined MVD in tissues based on CD34 expression in microvessels as a surrogate marker. The results demonstrated that the antitumor and anti-angiogenesis effects of osthole at the early and middle stages of HCC were similar. Additionally, there was a lack of CD34-positive microvessels

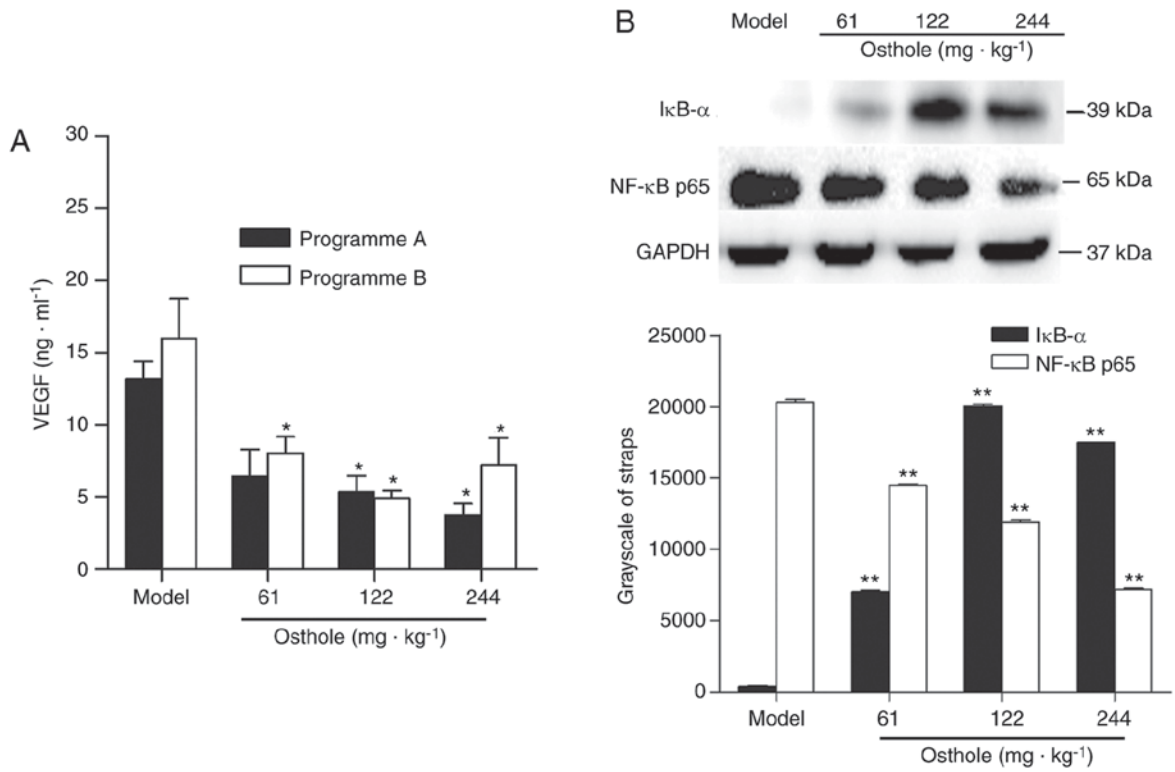

Figure 3. Effects of osthole on VEGF and NF-κB signaling in tumor tissues of orthotopic HCC-bearing mice. (A) Tumor tissues were collected following osthole treatment. Levels of VEGF in tumor tissues were measured by ELISA. (B) Protein expression of IκB-α and NF-κB p65 were detected by western blot analysis. Equal loading was confirmed by stripping immunoblots and reprobing for GAPDH. Statistical analysis of IκB-α and NF-κB p65 quantification. Data are represented as the mean ± standard error of the mean. *P<0.05, **P<0.01, compared with the model control group. VEGF, vascular endothelial growth factor; NF-κB, nuclear factor-κB; IκB-α, inhibitor of κB-α.

in normal liver tissue, while the tumor and adjacent tissues exhibited marked increases in CD34-MVDs, which was similar to a study undertaken by Dai *et al* (36). Furthermore, MVD was positively correlated with tumor weight, which supported the importance of angiogenesis for tumor growth. In order to grow beyond minimal size, tumors are required to induce the growth of angiogenesis; conversely, therapeutic inhibition of angiogenesis leads to inhibition of tumor growth (1,37). While the results from the correlation between MVD and tumor weight exhibited a low r-value. The small sample size and osthole treatment may have altered the r value obtained in the present study.

To date, whether osthole exerted anti-angiogenesis activity in HCC has remained largely unknown. In the present study, MVD in tumor and adjacent tissues was significantly decreased by treatment with osthole in a dose-dependent manner. Meanwhile, the expression of VEGF in tumor and adjacent tissues was markedly increased during tumor progression, but was significantly decreased by osthole administration. In addition, the results of the present study indicated that osthole inhibited the activity of NF-κB and decreased MVD in tumor and adjacent tissues, which is supported by previously published data demonstrating the importance of NF-κB in angiogenesis (38-42). To the best of our knowledge, the present study was the first to demonstrate the anti-angiogenesis efficacy of osthole, which may be, at least in part, responsible for its inhibition of tumor growth.

Anti-angiogenic approaches aimed at blocking vessel growth in cancer led to the approval of therapeutics targeting VEGF or VEGFR (8,18). The regulation of VEGF involves multiple signaling pathways (3). VEGF-C is the target gene of NF-κB and may enhance the binding capacity of NF-κB (20). In a previous study, following the activation of NF-κB, VEGF expression was increased and angiogenesis was promoted, and this in turn resulted in an increase in MVD (43). By contrast, NF-κB signaling blockade significantly inhibited the expression of the major pro-angiogenic molecules VEGF and interleukin-8 *in vitro* and *in vivo*, and thereby decreased MVD (44). The results of the present study demonstrated that the expression of NF-κB and VEGF in tumor and adjacent tissues was markedly increased during tumor progression, but was significantly decreased by osthole administration. This indicated that the mechanism involved in the anti-angiogenesis effect of osthole on HCC is associated with attenuation of the downregulation of NF-κB and VEGF. However, the present study did not provide further evidence linking the inhibitory effects of osthole on the angiogenesis with the NF-κB/VEGF signaling pathway, which represents a limitation of the current study. Further research is required to investigate the role of the NF-κB/VEGF signaling pathway in the inhibitory effects of osthole on angiogenesis *in vivo* and *in vitro* by pharmacological and genetic interference with NF-κB. In addition, NF-κB is involved in inflammatory responses, where it triggers the secretion of pro-inflammatory cytokines, and thereby induces VEGF secretion. Previous studies have observed that osthole interfered with the NF-κB signaling pathway during inflammation (45,46), which not only indicated the importance of the NF-κB signaling pathway to osthole-induced inhibition of angiogenesis, but also suggested that the anti-angiogenesis effect

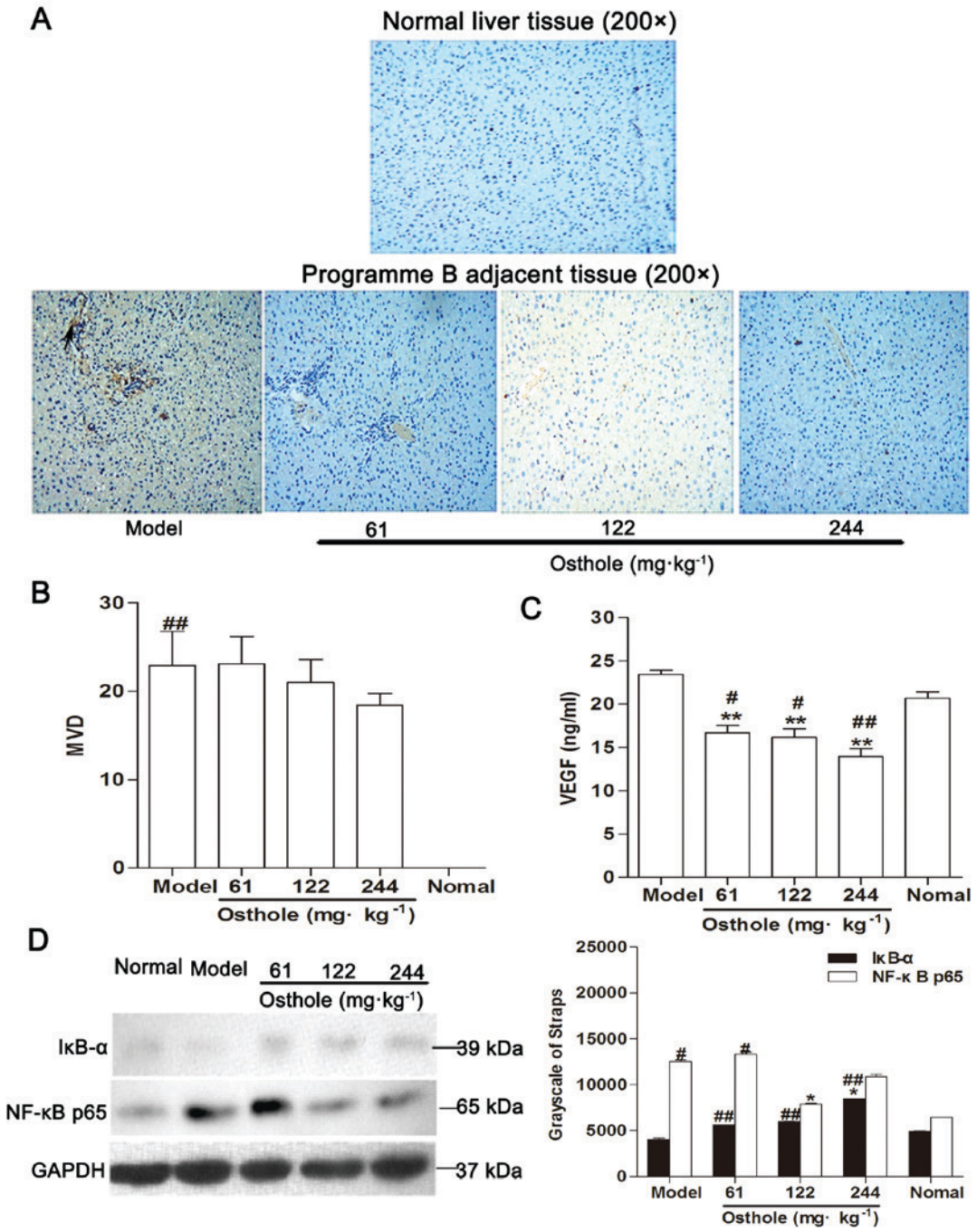

Figure 4. Effects of osthole on MVD, VEGF and NF-κB signaling in adjacent tissues of orthotopic hepatocellular carcinoma-bearing mice. (A) Immunohistochemical staining for blood vessels with CD34 (arrow) was performed on adjacent tissues from osthole-treated (61, 122 and 244 mg/kg) mice and normal liver tissue sections. (B) Compared with the model control group, the staining indicated that the MVD was decreased in the osthole-treated mice. (C) Expression levels of VEGF in adjacent tissues were measured by ELISA. (D) Adjacent tissue lysates were prepared and quantified. Protein expression of IκB-α and NF-κB p65 were detected by western blot analysis. Equal loading was confirmed by stripping immunoblots and reprobing for GAPDH. Statistical analysis of IκB-α and NF-κB p65 quantification. Data are presented as the mean ± standard error of the mean. *P<0.05, **P<0.01, compared with the model control group; $^{\#}$P<0.05, $^{\#\#}$P<0.01, compared with the normal control group. MVD, microvessel density; VEGF, vascular endothelial growth factor; NF-κB, nuclear factor-κB; IκB-α, inhibitor of κB-α.

of osthole is associated with the inhibition of inflammatory responses. Therefore, NF-κB may be the underlying mechanism of the inhibitory effects of osthole on the angiogenesis and inflammatory responses, which requires further study.

To the best of our knowledge, the present study was the first to demonstrate that osthole inhibited angiogenesis and tumor growth in mice bearing orthotopic HCC. The results of the present study indicated that osthole attenuates angiogenesis to inhibit the growth of HCC. Suppression of the NF-κB/VEGF signaling pathway may be, at least in part, involved in the anti-angiogenesis effect of osthole on HCC. In combination with our previous study, osthole exhibited antitumor effects through the induction of apoptosis, inhibition of angiogenesis and enhancement of antitumor immune responses, suggesting that it may be a promising leading compound for the treatment of HCC.

Acknowledgements

No applicable.

Funding

The present study was supported by the National Natural Science Foundation of China (grant no. 81303276), the Project Fund of Suzhou City (grant no. SYSD2015173) and research funds from the Suzhou Hospital of Traditional Chinese Medicine Youth Fund (grant no. YQN2014003).

Availability of data and materials

All data generated or analyzed during this study are included in this published article.

Authors' contributions

All authors contributed to the study concept and design, and the interpretation of the data. FY, LRZ, GRJ, ML, GQL and QY acquired and analyzed the data. FY, LRZ and GRJ drafted the manuscript. LRZ and GRJ reviewed the manuscript for important intellectual content. All authors revised the article and approved the final version for publication. LRZ is responsible for the integrity of the work as a whole.

Ethics approval and consent to participate

All the animal experimental procedures were conducted in compliance with the Directive 2010/63/EU. The study was approved by the Local Ethics Committee of Suzhou Hospital of Traditional Chinese Medicine (Suzhou, China).

Patient consent for publication

No applicable.

Competing interests

The authors declare that they have no competing interests.

References

1. Detmar M: Tumor angiogenesis. J Investig Dermatol Symp Proc 5: 20-23, 2000.
2. Yance DR Jr and Sagap SM: Targeting angiogenesis with integrative cancer therapies. Integr Cancer Ther 5: 9-29, 2006.
3. Zhao Y and Adjei AA: Targeting angiogenesis in cancer therapy: Moving beyond vascular endothelial growth factor. Oncologist 20: 660-673, 2015.
4. Yu HB, Zhang HF, Zhang X, Li DY, Xue HZ, Pan CE and Zhao SH: Resveratrol inhibits VEGF expression of human hepatocellular carcinoma cells through a NF-kappa B-mediated mechanism. Hepatogastroenterology 57: 1241-1246, 2010.
5. Rajabi M and Mousa SA: The role of angiogenesis in cancer treatment. Biomedicines 5: E34, 2017.
6. Berqers G and Hanahan D: Modes of resistance to anti-angiogenic therapy. Nat Rev Cancer 8: 592-603, 2008.
7. Li C, Liu T, Bazhin AV and Yang Y: The sabotaging role of myeloid cells in anti-angiogenic therapy: Coordination of angiogenesis and immune suppression by hypoxia. J Cell Physiol 232: 2312-2322, 2017.
8. Hillen F and Griffioen AW: Tumour vascularization sprouting angiogenesis and beyond. Cancer Metastasis Rev 26: 489-502, 2007.
9. Chouaib S, Messai Y, Couve S, Escudier B, Hasmim M and Noman MZ: Hypoxia promotes tumor growth in linking angiogenesis to immune escape. Front Immunol 3: 21, 2012.
10. McDonald PC, Chafe SC and Dedhar S: Overcoming hypoxia-mediated tumor progression: Combinatorial approaches targeting ph regulation, angiogenesis and immune dysfunction. Front Cell Dev Biol 4: 27, 2016.
11. Li Y and Martin RC II: Herbal medicine and hepatocellular carcinoma: Applications and challenges. Evid Based Complement Alternat Med 2011: 541209, 2011.
12. Yang LL, Wang MC, Chen LG and Wang CC: Cytotoxic activity of coumarins from the fruits of *Cnidium monnieri* on leukemia cell lines. Planta Med 69: 1091-1095, 2003.
13. Riviere C, Goossens L, Pommery N, Fourneau C, Delelis A and Henichart JP: Antiproliferative effects of isopentenylated coumarins isolated from phellolophium madagascariense baker. Nat Prod Res 20: 909-916, 2006.
14. Xu X, Zhang Y, Qu D, Jiang T and Li S: Osthole induces G2/M arrest and apoptosis in lung cancer A549 cells by modulating PI3K/Akt pathway. J ExpClin Cancer Res 30: 33-39, 2011.
15. Chou SY, Hsu CS, Wang KT, Wang MC and Wang CC: Antitumor effects of osthole from *Cnidium monnier*i: An in vitro and in vivo study. Phytother Res 21: 226-230, 2007.
16. Zhang L, Jiang G, Yao F, He Y, Liang G, Zhang Y, Hu B, Wu Y, Li Y and Liu H: Growth inhibition and apoptosis induced by osthole, a natural coumarin, in hepatocellular carcinoma. PLoS One 7: e37865, 2012.
17. Zhang L, Jiang G, Yao F, Liang G, Wang F, Xu H, Wu Y, Yu X and Liu H: Osthole promotes anti-tumor immune responses in tumor-bearing mice with hepatocellular carcinoma. Immunopharmacol Immunotoxicol 37: 301-307, 2015.
18. Potente M, Gerhardt H and Carmeliet P: Basic and therapeutic aspects of angiogenesis. Cell 146: 873-887, 2011.
19. Turlin B, Le Quilleuc D, Leroyer P, Brissot P, Deugnier Y and Loréal O: High vascular endothelial growth factor(VEGF) expression in chemically-induced hepatic microcancers in mice. J Hepatol 37: 620-624, 2002.
20. Tong Q, Zheng L, Lin L, Li B, Wang D, Huang C and Li D: VEGF is upregulated by hypoxia-induced mitogenic factor via the PI-3K/Akt-NF-kappaB signaling pathway. Respir Res 7: 37, 2006.
21. Zhang Q, Lu Y, Proulx ST, Guo R, Yao Z, Schwarz EM, Boyce BF and Xing L: Increased lymphangiogenesis in joints of mice with inflammatory arthritis. Arthritis Res Ther 9: R118, 2007.
22. Kwon OJ, Kim PH, Huyn S, Wu L, Kim M and Yun CO: A hypoxia- and {alpha}-fetoprotein-dependent oncolytic adenovirus exhibits specific killing of hepatocellular carcinomas. Clin Cancer Res 16: 6071-6082, 2010.
23. Wei D, Li Q, Wang XL, Wang Y, Xu J, Feng F, Nan G, Wang B, Li C, Guo T, *et al*: Oncolytic Newcastle disease virus expressing chimeric antibody enhanced anti-tumor efficacy in orthotopic hepatoma-bearing mice. J ExpClin Cancer Res 34: 153, 2015.
24. McFadden DG, Vernon A, Santiago PM, Martinez-McFaline R, Bhutkar A, Crowley DM, McMahon M, Sadow PM and Jacks T: p53 constrains progression to anaplastic thyroid carcinoma in a Braf-mutant mouse model of papillary thyroid cancer. Proc Natl Acad Sci U S A 111: E1600-E1609, 2014.
25. Meng J, Liu Y, Han J, Tan Q, Chen S, Qiao K, Zhou H, Sun T and Yang C: Hsp90β promoted endothelial cell-dependent tumor angiogenesis in hepatocellular carcinoma. Mol Cancer 16: 72, 2017.
26. Kim HY, Kim J, Ha Thi HT, Bang OS, Lee WS and Hong S: Evaluation of anti-tumorigenic activity of BP3B against colon cancer with patient-derived tumor xenograft model. BMC Complement Altern Med 16: 473, 2016.
27. Chen H, Zhang J, Luo J, Lai F, Wang Z, Tong H, Lu D, Bu H, Zhang R and Lin S: Antiangiogenic effects of oxymatrine on pancreatic cancer by inhibition of the NF-κB-mediated VEGF signaling pathway. Oncol Rep 30: 589-595, 2013.
28. Hui L and Chen Y: Tumor microenvironment: Sanctuary of the devil. Cancer Lett 368: 7-13, 2015.
29. Ribatti D and Vacca A: The role of microenvironment in tumor angiogenesis. Genes Nutr 3: 29-34, 2008.
30. Leenders MW, Nijkamp MW and Borel Rinkes IH: Mouse models in liver cancer research: A review of current literature. World J Gastroenterol 14: 6915-6923, 2008.
31. Rao Q, You A, Guo Z, Zuo B, Gao X, Zhang T, Du Z, Wu C and Yin H: Intrahepatic tissue implantation represents a favorable approach for establishing orthotopic transplantation hepatocellular carcinoma mouse models. PLoS One 11: e0148263, 2016.

32. Li B, Zhang Y, Wu W, Du G, Cai L, Shi H and Chen S: Neovascularization of hepatocellular carcinoma in a nude mouse orthotopic liver cancer model: A morphological study using X-ray in-line phase-contrast imaging. BMC Cancer 17: 73, 2017.
33. Woodfield SE, Shi Y, Patel RH, Jin J, Major A, Sarabia SF, Starosolski Z, Zorman B, Gupta SS, Chen Z, *et al*: A novel cell line based orthotopic xenograft mouse model that recapitulates human hepatoblastoma. Sci Rep 7: 17751, 2017.
34. Weidner N, Semple JP, Welch WR and Folkman J: Tumor angiogenesis and metastasis - correlation in invasive breast carcinoma. N Engl J Med 324: 1-8, 1991.
35. El-Assal ON, Yamanoi A, Soda Y, Yamaguchi M, Igarashi M, Yamamoto A, Nabika T and Nagasue N: Clinical significance of microvessel density and vascular endothelial growth factor expression in hepatocellular carcinoma and surrounding liver: Possible involvement of vascular endothelial growth factor in the angiogenesis of cirrhotic liver. Hepatology 27: 1554-1562, 1998.
36. Dai L, Peng XX, Tan EM and Zhang JY: Tumor-associated antigen CAPERα and microvessel density in hepatocellular carcinoma. Oncotarget 7: 16985-16995, 2016.
37. Cao Y and Langer R: A review of Judah Folkman's remarkable achievements in biomedicine. Proc Natl Acad Sci USA 105: 13203-13205, 2008.
38. Aggarwal BB, Vijayalekshmi RV and Sung B: Targeting inflammatory pathways for prevention and therapy of cancer: Short-term friend, long-term foe. Clin Cancer Res 15: 425-430, 2009.
39. Schmidt D, Textor B, Pein OT, Licht AH, Andrecht S, Sator-Schmitt M, Fusenig NE, Angel P and Schorpp-Kistner M: Critical role for NF-kappaB-induced JunB in VEGF regulation and tumor angiogenesis. EMBO J 26: 710-719, 2007.
40. Ismail HA, Lessard L, Mes-Masson AM and Saad F: Expression of NF-kappaB in prostate cancer lymph node metastases. Prostate 58: 308-313, 2004.
41. Ghosh S and Karin M: Missing pieces in the NF-kappaB puzzle. Cell 109 (Suppl): S81-S96, 2002.
42. Javan H, Szucsik AM, Li L, Schaaf CL, Salama ME and Selzman CH: Cardiomyocyte p65 nuclear factor-κB is necessary for compensatory adaptation to pressure overload. Circ Heart Fail 8: 109-118, 2015.
43. Zhang B, Wang D, Ji TF, Shi L and Yu JL: Overexpression of lncRNA ANRIL up-regulates VEGF expression and promotes angiogenesis of diabetes mellitus combined with cerebral infarction by activating NF-κB signaling pathway in a rat model. Oncotarget 8: 17347-17359, 2017.
44. Xiong HQ, Abbruzzese JL, Lin E, Wang L, Zheng L and Xie K: NF-kappaB activity blockade impairs the angiogenic potential of human pancreatic cancer cells. Int J Cancer 108: 181-188, 2004.
45. Yu C, Li P, Qi D, Wang L, Qu HL, Zhang YJ, Wang XK and Fan HY: Osthole protects sepsis-induced acute kidney injury via down-regulating NF-κB signal pathway. Oncotarget 8: 4796-4813, 2017.
46. Li YQ, Wang JY, Qian ZQ, Li YL, Li WN, Gao Y and Yang DL: Osthole inhibits intimal hyperplasia by regulating the NF-κB and TGF-β1/Smad2 signalling pathways in the rat carotid artery after balloon injury. Eur J Pharmacol 811: 232-239, 2017.